Atmospheric Blocking Trends and Seasonality around the Antarctic Peninsula

JULIO C. MARÍN,[a,b] DENIZ BOZKURT,[a,b,c,d] AND BRADFORD S. BARRETT[e]

[a] *Departamento de Meteorología, Universidad de Valparaíso, Valparaíso, Chile*
[b] *Centro de Estudios Atmosféricos y Astroestadística, Universidad de Valparaíso, Valparaíso, Chile*
[c] *Center for Climate and Resilience Research, Santiago, Chile*
[d] *Centro de Investigación Oceanográfica COPAS COASTAL, Universidad de Concepción, Concepción, Chile*
[e] *Oceanography Department, U.S. Naval Academy, Annapolis, Maryland*

(Manuscript received 23 April 2021, in final form 8 January 2022)

ABSTRACT: We analyze the seasonal evolution and trends of atmospheric blocking from 1979 to 2018 using a geopotential-height-based method over two domains, one located to the west (150°–90°W, 50°–70°S) and the other over and to the east (90°–30°W, 50°–70°S) of the Antarctic Peninsula. Spatial patterns of geopotential heights on days with blocking feature well-defined ridge axes over and west of much of South America, and days with the most extreme blocking (above the 99th percentile) showed upper-tropospheric ridge and cutoff low features that have been associated with extreme weather patterns. Blocking days were found to be more frequent in the first half of the period (1979–98) than the second (1999–2018) in all seasons in the west domain, whereas they seem to be more common over the eastern (peninsula) domain in 1999–2018 for austral winter, spring, and autumn, although these differences were not statistically significant. West of the Antarctic Peninsula, blocking days occur most frequently when the Antarctic Oscillation (AAO) is negative, whereas they are more frequent over the peninsula when the AAO is positive. We propose that our blocking index can be used to indicate atmospheric blocking affecting the Antarctic Peninsula, similar to how the Greenland blocking index has been used to diagnose blocking, its trends, and impacts over the Arctic.

KEYWORDS: Antarctica; Blocking; Reanalysis data; Seasonal variability; Trends

1. Introduction

Blocked atmospheric flows can be identified by the appearance of an upper-tropospheric ridge that deflects cyclones from their usual storm tracks (Rex 1950a,b; Rasmusson and Wallace 1983; Legras and Ghil 1985). Blocking often occurs when the jet stream at middle and high latitudes develops meanders (Häkkinen et al. 2011); these meanders can be caused by splits in the jet stream (Trenberth and Mo 1985; Wright 1994; Berrisford et al. 2007; O'Kane et al. 2013) and both anticyclonic and cyclonic Rossby wave breaking (Berrisford et al. 2007; Weijenborg et al. 2012; Woollings et al. 2008). The equivalent-barotropic (Davini et al. 2021) circulations that typically result from atmospheric blocking are linked to a shift in the state of the atmosphere from high to low kinetic energy as the jet-stream-level circulation slows (Tyrlis and Hoskins 2008), and that shift can even reverse typical midlatitude flow from westerly to easterly (Tibaldi and Molteni 1990; Scherrer et al. 2006; Scaife et al. 2010) as tropospheric circulation in blocked flows takes on an anomalous meridional character (Barnes and Hartmann 2010).

Blocked atmospheric flows can have significant impacts on surface weather. Blocking can trap an air mass equatorward of an anticyclone (Häkkinen et al. 2011) for several days or even weeks (Davini et al. 2021). These equatorward air mass intrusions can lead to severe droughts and heat waves in summer (Black et al. 2004; Dole et al. 2011; Pfahl and Wernli 2012; Schaller et al. 2018) and severe cold episodes in winter (Dole and Gordon 1983; Hoskins and Sardeshmukh 1987; Sillmann et al. 2011; Buehler et al. 2011). Blocking also transports moisture poleward, and extreme flow blocking has been linked to anomalous moisture transport into the Arctic high latitudes (Barrett et al. 2020). Moisture transport in the high latitudes has major consequences for surface ice mass balance (Mattingly et al. 2018; Neff 2018), and thus blocking is also linked to important elements of climate and climate change (Kennedy et al. 2016; Woollings et al. 2018; Nabizadeh et al. 2019).

Both Northern Hemisphere (Barriopedro et al. 2006) and Southern Hemisphere blocking have been studied (Trenberth and Mo 1985; Sinclair 1996; Berrisford et al. 2007; Wiedenmann et al. 2002; de Lima Nascimento and Ambrizzi 2002; Patterson et al. 2019). In the Northern Hemisphere, blocking extremes occur in both winter and summer (Barrett et al. 2020). The climatological maximum in Northern Hemisphere winter blocking days tends to occur over the North Atlantic/western Europe and North Pacific sectors (Häkkinen et al. 2011;Wachowicz et al. 2021); in summer, the maximum in Northern Hemisphere blocking tends to occur in eastern Europe and western Russia (Masato et al. 2013). In the Southern Hemisphere, studies suggest there are sectors where blocking tends to occur, but few studies have explored either the seasonality or trends in blocking. Trenberth and Mo (1985) found that Southern Hemisphere blocking tends to occur preferentially in three sectors: New Zealand, south and southeast of the Andes, and in the southern Indian Ocean. A climatology by Sinclair (1996) shows that blocked anticyclones in the Southern Hemisphere are more frequent in winter than summer, and the climatological maximum in both winter and summer seasons tends to cluster in the Western Hemisphere

Barrett's current affiliation: Air Force Office of Scientific Research, Santiago, Chile.

Corresponding author: J. C. Marín, julio.marin@meteo.uv.cl

DOI: 10.1175/JCLI-D-21-0323.1

between 180° and 90°W and between 40° and 80°S. Tibaldi et al. (1994) noted that Southern Hemisphere blocking tends to be "simpler" than Northern Hemisphere. They identified a single broad zone of blocking from 150°E to 70°W with two relative maxima: one in an Australian sector from 150°E to 150°W and another in an Andean sector from 100° to 70°W. Despite these studies, seasonality and long-term (40+ years) trends in Southern Hemisphere blocking remain as open questions.

Recent work has connected blocking in the Australian sector to significant societal impacts from drought and fires (Pook et al. 2013; Parker et al. 2014; Reeder et al. 2015). Over South America, Rodrigues and Woollings (2017) found blocking linked to anticyclonic wave breaking over subtropical South America, and those blocking events were found associated with extremes of temperature and precipitation. Given these impacts, it is critical to understand and identify trends in atmospheric flow blocking, and here we do so in the sectors surrounding the Antarctic Peninsula. We focus here because this region is influenced by baroclinic midlatitude systems, westerlies, and tropical and extratropical quasi-stationary wave trains, which in turn can lead to episodic regional circulation anomalies that are connected to important changes in the Antarctic Peninsula surface climate (e.g., Stammerjohn et al. 2008; Fogt et al. 2012; Clem and Fogt 2013; Turner et al. 2016; Yuan et al. 2018; Clem et al. 2021). We thus focus on blocking in latitude belts that include the Antarctic Peninsula, as surface pressure patterns there (particularly in the Amundsen–Bellingshausen Sea and Weddell Sea) have been linked to important sensible weather and cryospheric processes in both Antarctica and South America (Hirasawa et al. 2013; Hosking et al. 2013; Turner et al. 2016; Bozkurt et al. 2018; Carrasco et al. 2021; Rondanelli et al. 2019).

Many quantitative metrics have been developed to identify atmospheric flow blocking. Both hierarchical methods like spatial clustering (Cheng and Wallace 1993) and nonhierarchical methods like partitioning (Michelangeli et al. 1995) have been used, along with nonlinear equilibrium (Vautard 1990) and mixture-model methods (Smyth et al. 1999). Some of the more popular operational metrics involve measures of the strength of the westerly middle- and upper-tropospheric flow (LejenÄs and Økland 1983; Pelly and Hoskins 2003) and direction of the geopotential height (Tibaldi and Molteni 1990) and potential vorticity (Shutts 1986) gradients. Simpler metrics have been created for the Northern Hemisphere, and one of these, the Greenland blocking index (GBI) developed by Fang (2004) and popularized by Hanna et al. (2013, 2014, 2015), has enjoyed widespread adoption because of its ease of calculation, interpretation, and statistical associations with impactful surface weather patterns (Hanna et al. 2013, 2014, 2015, 2018; Barrett et al. 2020; Wachowicz et al. 2021).

In this study, two blocking indices extending across the high-latitude Southern Hemisphere from 150° to 30°W are developed by applying a method similar to that used to calculate the GBI. The goal is to provide, for perhaps the first time, simple metrics to capture blocking around southern South America and Antarctica. The remainder of this article is organized as follows: the data and methods used to calculate the blocking indices are presented in the next section. In the results section, we compare our method with the more sophisticated blocking index of Tibaldi (Tibaldi and Molteni 1990; Tibaldi et al. 1994) and show multidecadal trends and seasonalities of blocking days detected by our indices. A discussion of implications of the metrics follows, and the article ends with conclusions.

2. Data and methods

a. Data

We define blocking indices in two spatial domains (defined below) using gridded data from the European Center for Medium-Range Weather Forecasts (ECMWF) interim reanalysis (ERA-Interim; Dee et al. (2011)) at 0.75° × 0.75° latitude–longitude grid over the 40-yr period January 1979 to December 2018. For each day in the 40-yr period, we analyzed 1200 UTC geopotential height at 500 hPa. We selected the ERA-Interim reanalysis because it has been shown to yield overall good results in capturing general circulation patterns and surface climate characteristics at higher latitudes in the Southern Hemisphere (Bromwich et al. 2011; Bracegirdle 2013; Jones et al. 2016; Tang et al. 2018). We also compared mean geopotential heights at 500 hPa between ERA-Interim and the more recent ERA5 dataset in the region of analysis and found an almost perfect match, supporting the use of ERA-Interim in this synoptic-scale study. In addition, our choice of ERA-Interim facilitates comparisons with previous studies using similar resolutions (Gonzalez et al. 2018).

We also analyzed blocking using the methods of Tibaldi and Molteni (1990) and Tibaldi et al. (1994) for the Southern Hemisphere to place our definition of *extreme* blocking in context with other studies on blocking. In addition, Gonzalez et al. (2018) created a daily series of the atmospheric synoptic patterns present each day in a domain around the Antarctic Peninsula from 1 January 1979 to 31 December 2016. They used a cluster analysis and visual inspection to select the five synoptic patterns that better represent the large-scale conditions over the region. We use the daily time series from Gonzalez et al. (2018) to examine the synoptic clusters present during blocking. Finally, since atmospheric flow blocking is favored when the jet stream is less zonal and weaker (Ndarana and Waugh 2011), such as what occurs during the negative phase of the AAO (Wallace 2000; Thompson and Wallace 2000), we also compare blocking over our region of interest with the AAO for the period 1979–2018. For that calculation, we used the daily values of the NOAA Climate Prediction Center AAO index (Mo 2000).

b. Methods

A number of methods have been described in the literature to define atmospheric blocking. A review of them can be found in Woollings et al. (2018). As mentioned by Patterson et al. (2019), most methods look for persistent positive geopotential height or surface pressure anomalies, or they look at persistent reversals of potential vorticity or geopotential height gradients. In this study, we quantified blocking in two different longitude–latitude domains of 60° × 20° in size: our first domain is located to the west of the Antarctic Peninsula

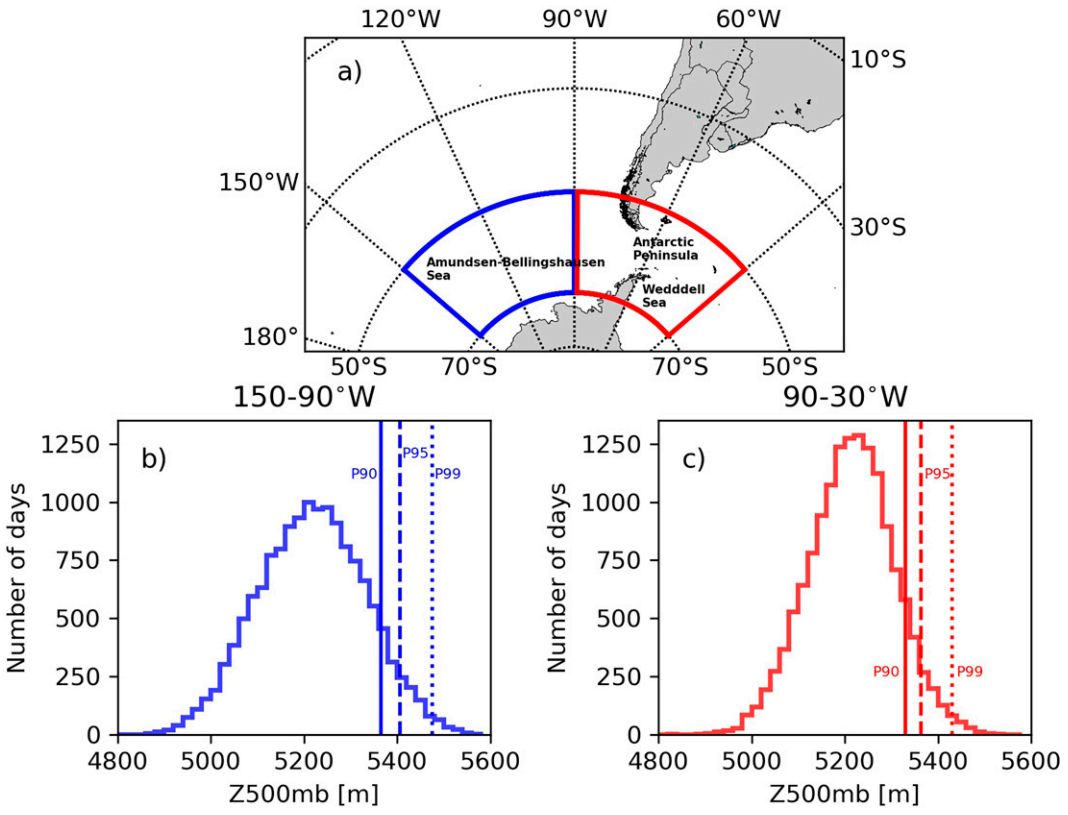

FIG. 1. (a) Map showing the two domains (blue and red boxes) for which blocking was analyzed in this study. The blue coloring for the domain 150°–90°W, 50°–70°S and the red coloring for the domain 90°–30°W, 50°–70°S are the same through the remainder of the figures. Also shown is the distribution of 500-hPa mean geopotential heights averaged over the (b) 150°–90°W and (c) 90°–30°W domains. Vertical lines in (b) and (c) show the values of 90th, 95th, and 99th percentiles, as marked.

(150°–90°W, 50°–70°S), and the second domain is located over and to the east (90°–30°W, 50°–70°S) of the peninsula (Fig. 1a). Note that we also compared a smaller domain (70°–30°W) to examine blocking to the west and east of the Antarctic Peninsula. We present the results of the larger domain here (which includes the peninsula) because they were similar to the smaller one located only to the east of the peninsula. We selected these two domains to be consistent with previous studies on important synoptic characteristics of the region, such as pressure centers in the Amundsen–Bellingshausen Sea and the Weddell Sea (King and Turner 2009; Hosking et al. 2013; Oliva et al. 2017; Gonzalez et al. 2018; Bozkurt et al. 2020).

Given that internal variability of the regional atmospheric circulation patterns around the Antarctic Peninsula can lead to important decadal variability, we subdivide the 40-yr period into two periods: 1979–98 and 1999–2018. For instance, recent studies show that temperature records for the Antarctic Peninsula over the last three decades shifted from a warming trend during 1979–97 to a cooling trend during 1999–2014 (Turner et al. 2016; Oliva et al. 2017; Carrasco et al. 2021), and that shift seems to be associated with more cyclonic conditions in the northern Weddell Sea (Turner et al. 2016). In addition, a phase change of the interdecadal Pacific oscillation from positive to negative was observed in the late 1990s (Meehl et al. 2016), and this could impact blocking over our domains. In addition to guidance from the blocking climatologies of Sinclair (1996) and Tibaldi et al. (1994), our choice of blocking regions considers the analysis of Gonzalez et al. (2018). Gonzalez et al. (2018) identified the major synoptic patterns around the Antarctic Peninsula using sea level pressure fields and cluster analysis over 45°–75°S, 120°–20°W, and they found five dominant patterns: low over the Weddell Sea (LWS), low over the Amundsen and Bellingshausen Seas (LAB), low over the Drake Passage (LDP), zonal flow over the Drake Passage (ZDP) and ridge over the Antarctic Peninsula (RAP). In this study, we place our blocking results within the context of these five synoptic clusters.

Our blocking indices were created by calculating the mean 500-hPa geopotential height averaged over each spatial domain (Figs. 1b,c), resulting in two daily time series of blocking, one for each spatial domain. We defined "extreme blocking" as a day when the mean 500-hPa height value was greater than the 90th percentile value (P90), similar to the method that Barrett et al. (2020) developed for Greenland. "Very extreme blocking" days were defined when heights exceeded the 95th (P95) and 99th (P99) percentiles, again following Barrett et al. (2020). Blue and red vertical lines in Figs. 1b and 1c show the values of P90 (solid

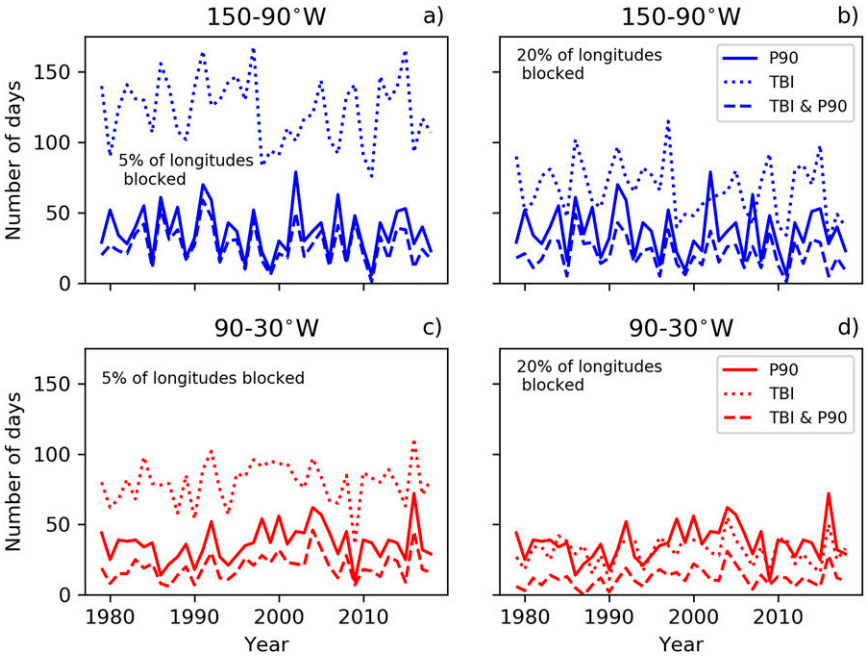

FIG. 2. Annual number of extreme blocking days (P90), the number of blocking days detected by Tibaldi's method (TBI), and the number of days that were detected by both our method and Tibaldi's method (TBI and P90) when (left) 5% and (right) 20% of domain longitudes in TBI are blocked for (a),(b) the domain 150°–90°W and (c),(d) the domain 90°–30°W between 1979 and 2018.

lines), P95 (dashed lines), and P99 (dotted lines) of the geopotential height distributions for domains 150°–90°W and 90°–30°W, respectively. Percentile thresholds were also calculated separately for summer (December–February: DJF), autumn (March–May: MAM), winter (June–August: JJA) and spring (September–November: SON), and the total number of extreme and very extreme blocking days in each year was obtained by adding the days in each season that exceeded the respective threshold. We analyzed and contrasted the seasonality and trends of P90, P95, and P99 blocking days for both domains. Furthermore, we also analyzed the persistence of blocking events of different duration, and here we tested events with 2+ and 4+ consecutive days with geopotential heights above the P90 and P95 (P99 behaved similarly to P95, so it is not shown).

As stated in section 2, we compared our indices with the blocking definition developed by Tibaldi and Molteni (1990) and Tibaldi et al. (1994) for the Southern Hemisphere. The Tibaldi blocking index (hereinafter TBI) determines whether blocking is present along a particular line of longitude by analyzing the 500-hPa geopotential height gradient reversal between 30° and 70°S. If the height gradient reverses along a longitude, that longitude line is classified as blocked by TBI. Since we are analyzing blocking over two domains and not just single longitude lines (Fig. 1a), we compared the number of blocking days obtained by our method with those obtained using TBI by varying the percentage of longitude lines in each domain that needed to be marked as blocked according to TBI.

3. Results

In this section, we first compare our method with TBI. Then, we present seasonality and trends of blocking days and events. Last, we relate blocking with the AAO.

a. Comparison with TBI

Figures 2a and 2c show that the total number of blocking days detected by the TBI method (dotted lines) was larger than the number of P90 blocking days detected by our method (solid lines) in both the 150°–90°W and 90°–30°W domains when 5% of domain longitudes were blocked according to TBI (Figs. 2a,c). The differences between the two methods are more pronounced over the 150°–90°W domain than the 90°–30°W domain (cf. Fig. 2a with Fig. 2c). The agreement between the total number of blocking days detected by TBI and our method (P90) increases when we consider a greater fraction of longitudes blocked according to TBI (Figs. 2b,d, when 20% of longitudes are blocked). This makes sense, considering that a synoptic-scale blocking pattern would tend to cover an extensive area, and we consider blocking over 60° swaths.

As the number of longitude lines with TBI blocking increases, the fraction of days with blocking in both our method and TBI decreases (Table 1; Fig. 2). For example, 74.5% of days with P90 blocking in the western domain (150°–90°W) also have TBI blocking on at least 5% of longitude lines, but only 57.8% of days with P90 blocking also have TBI blocking on 20% of longitude lines (Table 1). That tendency is also seen at the P95 and

TABLE 1. Climatological (1979–2018) fraction of days that feature both P90, P95, and P99 blocking (from our method) and TBI blocking, when 5%, 10%, and 20% of longitudes are blocked.

Region	150°–90°W			90°–30°W		
Percent of longitudes blocked according to TBI (%)	5	10	20	5	10	20
Days with P90 blocking that also have TBI blocking (%)	74.5	69.9	57.8	54.4	48.2	32.2
Days with P95 blocking that also have TBI blocking (%)	80.7	76.9	66.5	62.2	56.2	40.4
Days with P99 blocking that also have TBI blocking (%)	88.1	86.1	77.5	77.5	74.2	56.3

P99 levels, as well as at all blocking thresholds (P90, P95, and P99 and 5%, 10%, and 20%) in the eastern domain (90°–30°W). The interannual variability in the number of days with extreme blocking (P90) and the number of same days also detected with TBI (when 5% of domain longitudes were blocked) also agree well, even though our method tends to yield a slightly larger number of days each year with extreme blocking (Figs. 2a,c).

Both the climatological and interannual agreements between our method (P90, P95, and P99) and TBI for the number of days detected by both methods appear to be weaker in the eastern domain than in the western domain (Table 1; Fig. 2). Nonetheless, the annual number of P90 blocking days is moderately correlated (correlation coefficients ranging between 0.40 and 0.45) with the number of total days of TBI blocking (using any of the longitude thresholds 5%, 10%, and 20%) in the 150°–90°W domain, whereas the interannual agreement is even higher in the eastern domain (90°–30°W), with correlation coefficients between 0.64 and 0.70.

The mean 500-hPa geopotential height field on days with extreme blocking (P90, P95, and P99) is very similar to the mean height field on days with TBI blocking (when 20% of domain longitudes are blocked), for each domain (Fig. 3). However, blocking days obtained from our method feature a more intense ridge pattern than those in TBI. This is because our method detects blocking when the largest geopotential heights are present, whereas TBI could indicate blocking on days when geopotential heights are not as high. The more intense ridge pattern obtained by our method is most notable on the P99 days, and on those days the ridge extends all the way from the southern subtropics toward the Amundsen–Bellingshausen Sea (western

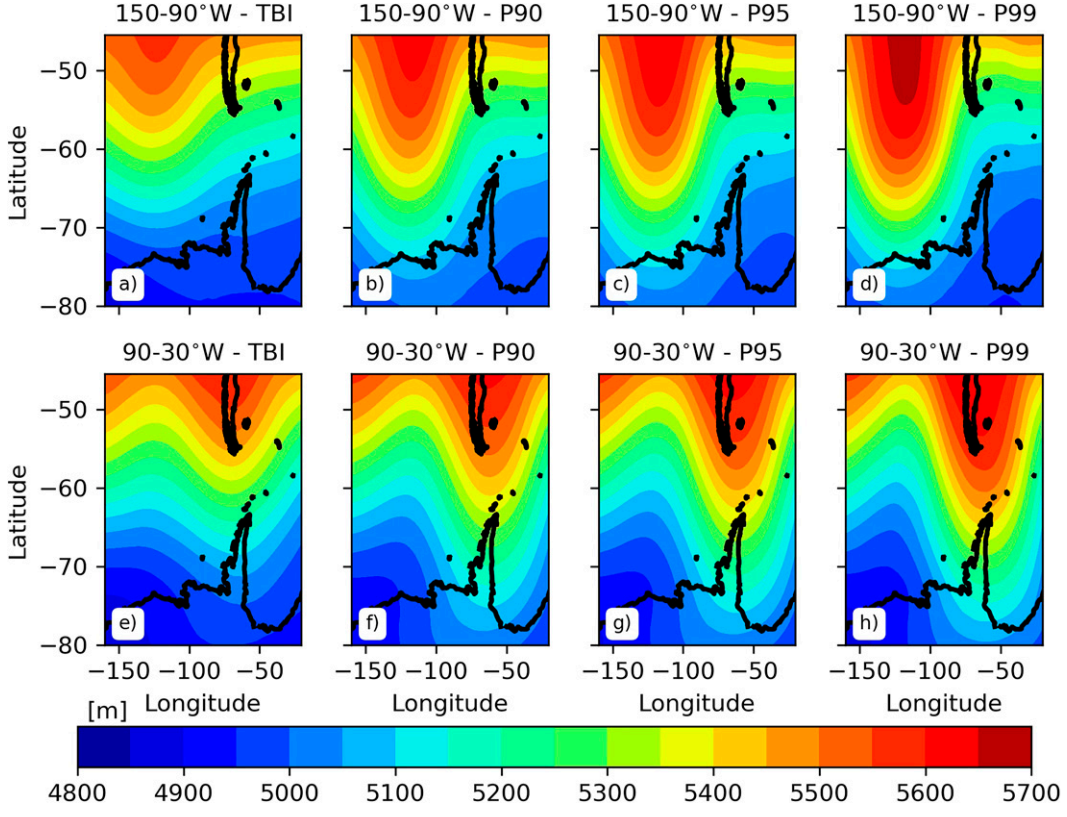

FIG. 3. Spatial distribution of mean 500-hPa geopotential heights averaged over all blocking days obtained from (left) Tibaldi's method (TBI, when 20% of domain longitudes are blocked) and from our method for (left center) P90, (right center) P95, and (right) P99 for (a)–(d) the domain 150°–90°W and (e)–(h) the domain 90°–30°W over the period 1979–2018.

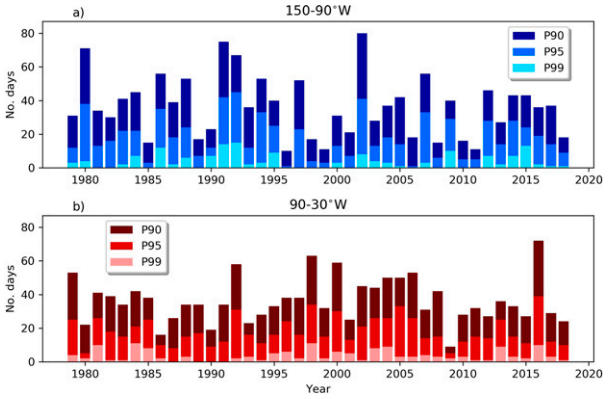

FIG. 4. Interannual variability in the number of blocking days by extremity of the blocking index above the 90th (P90), 95th (P95), and 99th (P99) percentiles for the period 1979–2018 for (a) the 150°–90°W domain and (b) the 90°–30°W domain.

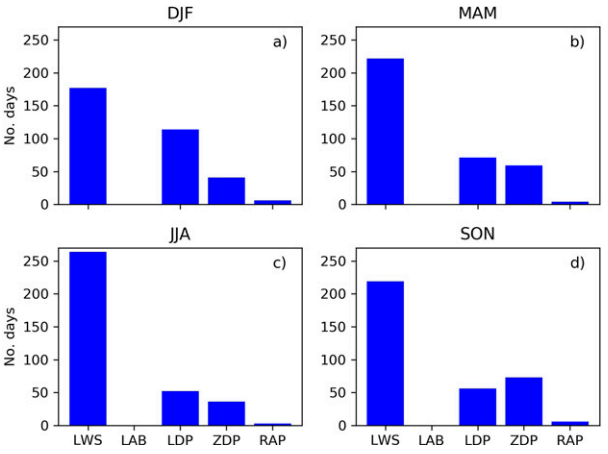

FIG. 5. Total number of (a) DJF, (b) MAM, (c) JJA, and (d) SON extreme blocking (P90) days (1979–2018) for the 150°–90°W domain associated with each synoptic classification developed by Gonzalez et al. (2018). The synoptic patterns are as follows: low over the Weddell Sea (LWS), low over the Amundsen and Bellingshausen Seas (LAB), low over the Drake Passage (LDP), zonal flow over the Drake Passage (ZDP), and ridge over the Antarctic Peninsula (RAP).

domain) and the Antarctic Peninsula (eastern domain) (Figs. 3d,h). This difference in geopotential heights supports our choice to refer to blocking in our index as *extreme*.

The mean height field differences between the methods may be partly related to their definitions. For example, Tibaldi et al. (1994) calculates blocking along each longitude separately, whereas our method defines blocking when the domain-averaged value is above a certain threshold (>90th, 95th, and 99th percentiles). In addition, TBI detects blocking within the latitudinal range from 30° to 70°S, whereas our method analyzes a narrower latitudinal range (50°–70°S).

Overall, despite some differences between the methods, they still show notable agreement. Furthermore, the simplicity of our method supports its use in the analysis of blocking episodes near the Antarctic Peninsula, similar to the applicability of the GBI (Fang 2004), which has been used to analyze both long-term and instantaneous blocking episodes over Greenland (Davini et al. 2012, 2014). Therefore, we present blocking obtained from our method through the remainder of the results.

b. *Seasonality and trends in blocking days*

Figure 4 shows the interannual variability in the number of days with P90, P95, and P99 blocking over each domain for the period 1979–2018. Both domains exhibit large interannual variability in blocking, with some years featuring many days with blocking (up to 80) while some others featuring relatively few (fewer than 10). Larger interannual variability of blocking is evident over the 150°–90°W domain than over the 90°–30°W domain. In addition, individual years with many anomalous blocking days (e.g., 1980, 1991, 1992, and 2002) tend to be more frequent for the 150°–90°W domain than for the 90°–30°W domain. This is in agreement with several previous studies that have shown large geopotential height variability (Renwick 2002; Ding et al. 2012; Raphael et al. 2016) and the presence of persistent anticyclones in the 150°–90°W domain (Renwick 1998, 2005). When looking at annual changes in the number of P90, P95, and P99 days, a Mann–Kendall test did not show any statistically significant long-term trend in either the 150°–90°W or the 90°–30°W domain. The analysis of trends by season is discussed below.

We determined the most frequent synoptic patterns associated with P90 days in both domains using the daily synoptic classification developed for the Antarctic Peninsula region by Gonzalez et al. (2018). It is important to note that each blocking day corresponds to only one synoptic pattern. Figure 5 shows that LWS, corresponding to a ridge to the west of the Antarctic Peninsula (Gonzalez et al. 2018, their Figs. 2 and 3), is the most frequent synoptic configuration associated with days with P90 extreme blocking in the 150°–90°W domain during all seasons. The LWS pattern is even more prominent in MAM, JJA, and SON (Figs. 5b–d). In addition, LDP and ZDP are also related, although less frequently, to blocking, corresponding to a ridge farther to the west and northwest, respectively, of the Antarctic Peninsula.

Gonzalez et al. (2018) found that all five synoptic patterns presented a similar annual frequency of occurrence over their 38-yr period of study (1979–2016). However, they showed some differences by season. The LDP was the most frequent pattern to occur in DJF (28.9%), almost doubling the frequency of occurrence shown by the LWS pattern in DJF (16.5%). Thus, even though the LDP pattern occurs twice as often as the LWS pattern in DJF (see their Table 1), blocking in the 150°–90°W domain is more common during the LWS synoptic pattern. On the other hand, despite the LWS pattern occurring slightly more often (23%) than the LDP pattern (17.5%) during JJA (see their Table 1), almost all the ridging west of the Antarctic Peninsula occurs during the LWS synoptic pattern in that season (Fig. 5c). Similar results were found for SON and MAM in the 150°–90°W domain, whereby blocking was most common when a low pressure was located in the Weddell Sea (LWS pattern).

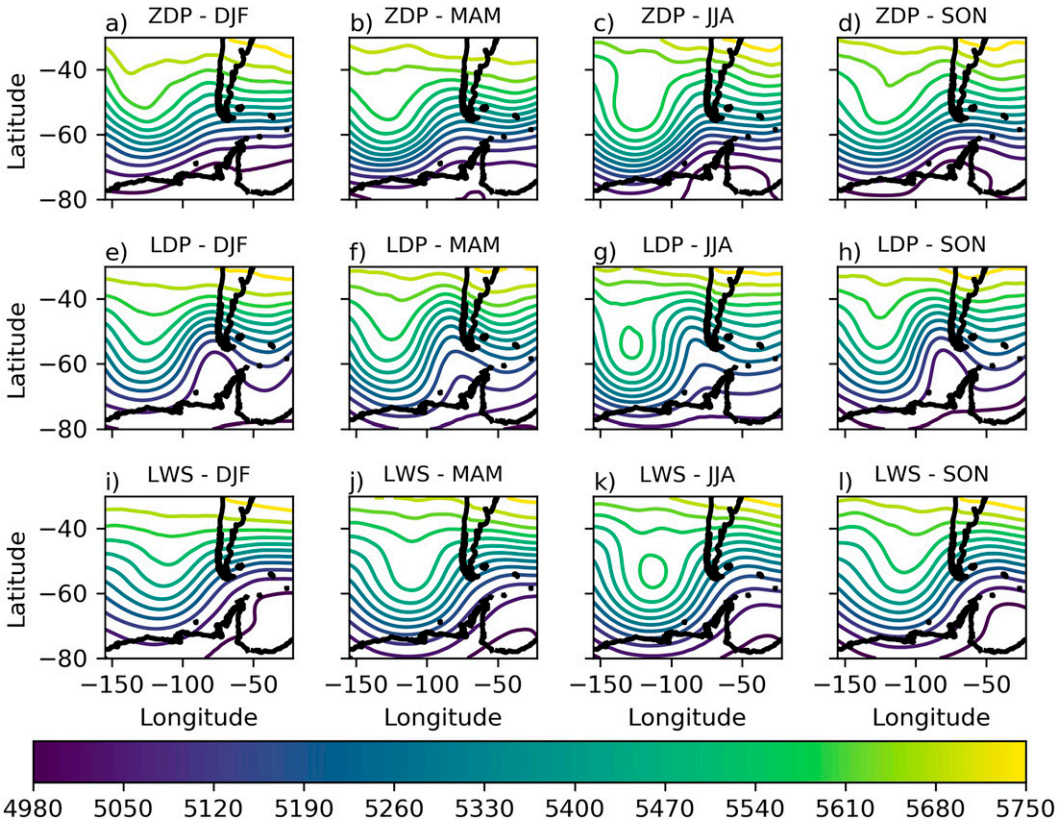

FIG. 6. Spatial distribution of mean seasonal 500-hPa geopotential height for P90 days associated with (a)–(d) the low over the Drake Passage (LDP) synoptic pattern, (e)–(h) the low over the Weddell Sea (LWS), and (i)–(l) the zonal flow over the Drake Passage (ZDP) synoptic pattern over the 150°–90°W domain for the period 1979–2018. The LDP, LWS, and ZDP synoptic classification is developed by Gonzalez et al. (2018).

The spatial distribution of seasonal mean 500-hPa geopotential heights averaged over the P90 days associated with the ZDP, LDP, and LWS patterns for the 150°–90°W domain is shown in Fig. 6. As previously mentioned, the three synoptic patterns are associated with the presence of a midlevel ridge completely (LWS) or partially (LDP and ZDP) covering the 150°–90°W domain during the eastward movement of midlevel troughs and ridges through the region. Since a midlevel ridge completely covers the domain during an LWS pattern, area-averaged geopotential heights (values used in our indices) will be consistently larger than those calculated when the other patterns are present, resulting in more blocking days associated with the LWS over the 150°–90°W domain. Examples of the spatial distribution of 500-hPa geopotential heights for the P90 days with the highest value in DJF and MAM over the 150°–90°W domain, associated with the LWS synoptic pattern, are shown in Figs. 7a and 7b, respectively. They show a pronounced extratropical midtroposphere ridge located over the western domain, bounded by midtroposphere lows to its northeast and northwest sides.

The same pattern analysis for the 90°–30°W domain shows that RAP and LAB are the most frequent synoptic patterns associated with extreme blocking (P90) in our eastern domain (Fig. 8). Both of these synoptic patterns correspond to ridging conditions over and to the east of the Antarctic Peninsula. Blocking occurs more often over this domain during the RAP synoptic pattern than the LAB synoptic pattern in DJF, MAM, and JJA (Figs. 8a–c), whereas blocking is more frequent during the LAB synoptic pattern in SON (Fig. 8d). These results agree with Gonzalez et al. (2018) in terms of the frequency of both synoptic patterns by season (see their Table 1).

Figure 9 shows the spatial distribution of seasonal mean 500-hPa geopotential heights averaged over the P90 days associated with the RAP and LAB synoptic patterns for the 90°–30°W domain. The RAP and LAB patterns are associated with midlevel ridges whose axes are located immediately to the west and east of the Antarctic Peninsula, respectively. Examples of the spatial distribution of 500-hPa geopotential heights for the P90 days with the highest value over the 90°–30°W domain are associated with the RAP pattern in JJA and with the LAB synoptic pattern in SON (Fig. 7). The geopotential height distribution for JJA resembles a Rex block pattern (Rex 1950a) in which a midlevel ridge is located poleward of a midlevel low (Fig. 7c), whereas SON seems to feature an omega block pattern (Fig. 7d).

As previously mentioned, internal variability of regional atmospheric circulation patterns leads to important decadal variabilities, particularly in the temperature field. For instance, Bozkurt et al. (2020) showed that the recent cooling trend

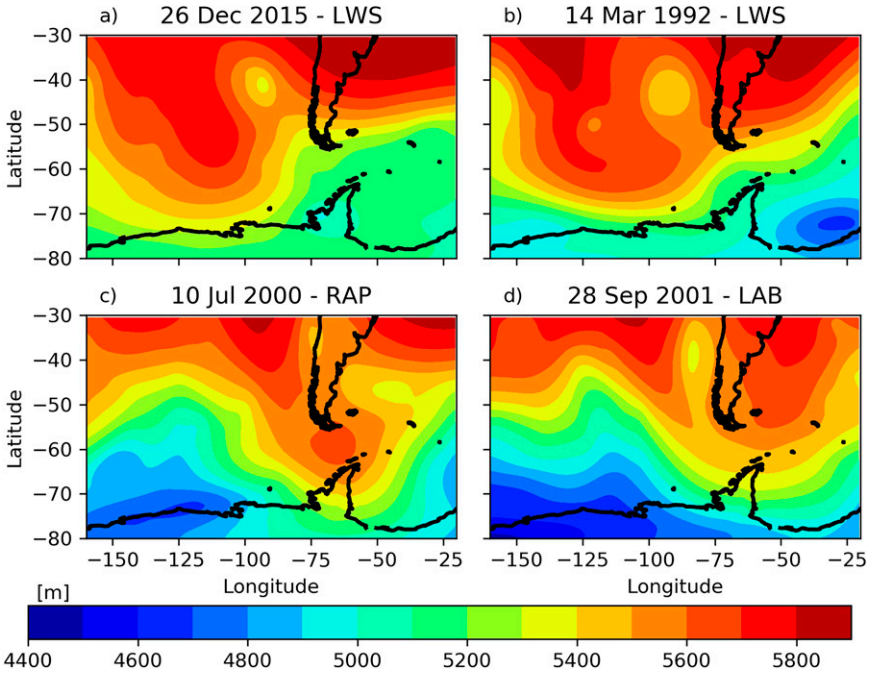

FIG. 7. Spatial distribution of geopotential height for P90 days with the highest value in (a) DJF and (b) MAM associated with the low over the Weddell Sea (LWS) synoptic pattern for the 150°–90°W domain for the period 1979–2018. (c) As in (a), but for JJA associated with the ridge over the Antarctic Peninsula (RAP) for the 90°–30°W domain for the period 1979–2018. (d) As in (c), but for SON associated with the low over the Amundsen and Bellingshausen Seas (LAB) for the 90°–30°W domain for the period 1979–2018. The LWS, RAP, and LAB synoptic classification is developed by Gonzalez et al. (2018).

over the Antarctic Peninsula (1999–2014) is dominated by a notable summer cooling trend triggered by the strengthening of the Weddell Sea low as well as trend toward more anticyclonic (northerly winds) over the Amundsen Sea (similar to the 150°–90°W domain in this work). Therefore, we first analyzed the changes in the mean 500-hPa geopotential heights averaged over each domain between the 1979–98 and 1999–2018 periods using a Kolmogorov–Smirnov test. We then contrasted differences between these subperiods with the long-term (1979–2018) trend.

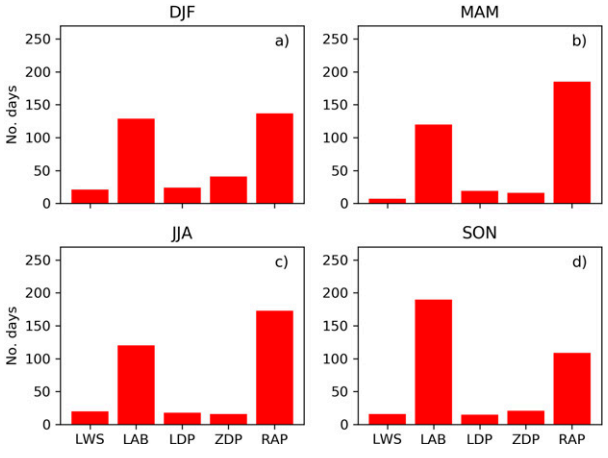

FIG. 8. As in Fig. 5, but for number of days with extreme blocking (P90) for the 90°–30°W domain.

The distributions of daily mean geopotential heights from 1979–98 and 1999–2018 for the 150°–90°W domain are statistically significantly different from each other. When we looked at the distributions of geopotential height for those two 20-yr periods by season (Table 2), they were statistically significantly different from each other in DJF, MAM, and JJA. The same analysis, but for the 90°–30°W domain, only found statistically significant differences in the geopotential height distributions for DJF.

We used a Mann–Kendall test to determine long-term trends in the annual mean 500-hPa geopotential height, averaged over the 150°–90°W and 90°–30°W domains for the period 1979–2018. We did not find statistically significant trends for either of the domains. The p values of the Mann–Kendall test calculated by season (Table 3) only showed a slight statistically significant decreasing trend for DJF over the 90°–30°W domain for the period 1979–2018. Thus, the mean geopotential height around the peninsula does not seem to exhibit statistically significant trends over the period 1979–2018. However, we did find significant differences between the first and second 20-yr periods, and as we highlight below, we believe this is indicative of *multidecadal* variability.

The frequency in the number of days with extreme blocking (P90) by season shows changes from the first (1979–98) to the

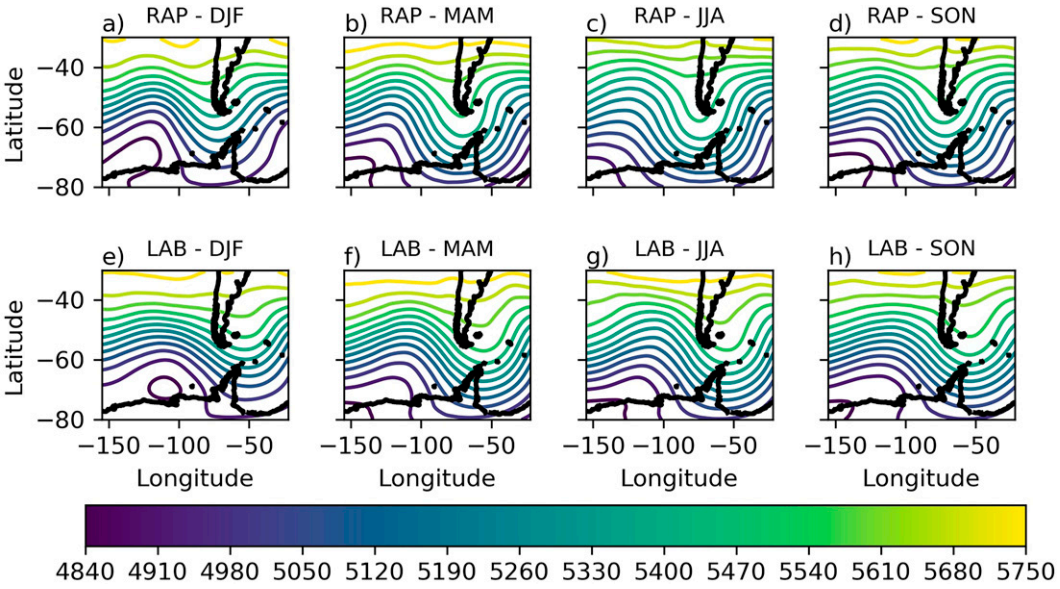

FIG. 9. Spatial distribution of mean 500-hPa geopotential height for P90 days associated with the Ridge over the Antarctic Peninsula (RAP) synoptic pattern over the 90°–30°W domain during (a) DJF, (b) MAM, (c) JJA, and (d) SON and for 1979–2018. (e)–(h) As in (a)–(d), but for the low over the Amundsen and Bellingshausen Seas (LAB) synoptic pattern. The RAP and LAB synoptic classification is developed by Gonzalez et al. (2018).

second period (1999–2018) in both domains (Figs. 10 and 11). The number of days with blocking (P90) tends to decrease in the 1999–2018 period during all seasons over the 150°–90°W domain, as can be seen in Table 4. The largest decreases occur in MAM and JJA (Figs. 10b,c). On the other hand, DJF and SON show little decrease, yet increases of the extremes in the right tail (~>5500 m) are indicated during the second period (Figs. 10a,d). Note that, relative to the frequency of P90, the frequency of very extreme blocking (P99) yields larger increases in DJF and SON during the second period (see Table 4). On the contrary, notable decreases in blocking are evident in the right tail (~>5450 m) during the second period in MAM. In agreement with this signal, MAM and JJA also exhibit the largest decrease in the frequency of days with very extreme blocking (P99) during the second period (Table 4). None of the changes in the number of days with extreme blocking between the two 20-yr periods over the 150°–90°W domain was statistically significant (using a Kolmogorov–Smirnov test).

Unlike the 150°–90°W domain, the frequency of blocking days over the 90°–30°W domain tends to decrease in DJF during the second period, particularly toward the right tail (~>5400 m) (Fig. 11a and Table 5). At the P99 level, very extreme blocking in DJF was 2.5 times more common in the first two decades than in the last two (Table 5). In contrast with DJF, days with blocking tend to be more common in MMA, JJA, and SON in the second period than the first. In particular, the frequency of days with the most extreme blocking (P99) for MAM in the second period is about 2 times that in the first period (Table 5). Despite consistent changes in the P90, P95, and P99 seasonal distributions between both periods over the 90°–30°W domain, Kolmogorov–Smirnov tests showed that they were not statistically significant.

Variability in the frequency of blocking was also reported by Wachowicz et al. (2021), who found meaningful trends in blocking by season over the Northern Hemisphere and urged that trends in blocking be considered by season and not in yearly aggregates. Gonzalez et al. (2018) also found a positive trend (significant at 95%) in the frequency of LAB patterns in MAM, which is one of the two synoptic patterns associated with ridging in the 90°–30°W domain. In our case, long-term (1979–2018) trends (using a Mann–Kendall test) in blocking

TABLE 2. The p values of the Kolmogorov–Smirnov tests applied to the distributions of mean 500-hPa geopotential heights for the 1979–98 and 1999–2018 periods and for both domains of study.

Seasons	150°–90°W	90°–30°W
DJF	0.016	9.36×10^{-11}
MAM	6.16×10^{-7}	0.43
JJA	0.013	0.64
SON	0.42	0.21

TABLE 3. The p values of the Mann–Kendall test to estimate statistically significant trends in the annual number of blocking days (P90) over the 1979–2018 period for both domains of study.

Seasons	150°–90°W	90°–30°W
DJF	0.7	0.003
MAM	0.2	0.74
JJA	0.45	0.97
SON	0.4	0.65

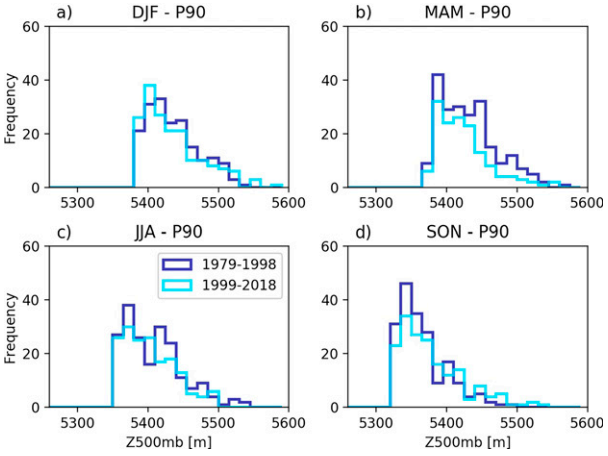

FIG. 10. Histogram of frequency of (a) DJF, (b) MAM, (c) JJA, and (d) SON extreme blocking (P90) for the first (1979–98; dark blue) and second (1999–2018; light blue) periods for the domain 150°–90°W.

days were not statistically significant for any domain nor season of analysis.

c. *Seasonality and trends in blocking events*

As discussed by Woollings et al. (2018), objective methods can determine local and instantaneous blocking conditions on gridded fields. They use criteria for spatial extension, stationarity, and persistence of blocking (usually around 4 days). In addition to defining blocking using instantaneous values (P90, P95, and P99), we also analyzed persistence of blocking *events*, here defined as consecutive P90, P95, and P99 days.

We selected six groups of blocking events. The first three groups comprise events with at least two consecutive days with geopotential heights above the P90, P95, and P99 levels (2+ consecutive days), respectively; the last three groups comprise events with at least four consecutive days with heights above the P90, P95, and P99 levels (4+ consecutive days), respectively. It is important to note that the sample size of blocking events with consecutive P99 days was small, particularly for events with 4+ consecutive days. Therefore, the discussion of results is mostly focused on events with days with consecutive blocking above P90 and P95.

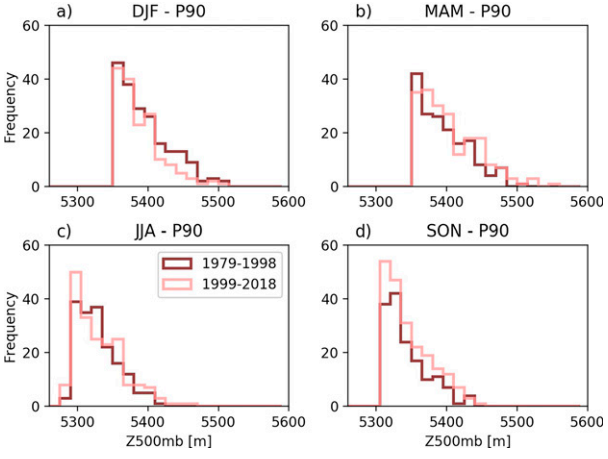

FIG. 11. Histogram of frequency of (a) DJF, (b) MAM, (c) JJA, and (d) SON extreme blocking (P90) for the first (1979–98; dark red) and second (1999–2018; light red) periods for the domain 90°–30°W.

TABLE 4. Percent of days with P90, P95, and P99 blocking over the 150°–90°W domain for the 1979–98 and 1999–2018 periods.

	1979–98			1999–2018		
Season percentile	P90	P95	P99	P90	P95	P99
DJF	50.7	53.6	43.2	49.3	46.4	56.8
MAM	59.8	64.7	67.6	40.2	35.3	32.4
JJA	53.8	57.6	64.9	46.2	42.4	35.1
SON	51.6	45.6	32.4	48.4	54.4	67.6

As expected, the correlation between the annual number of events of 2+ and 4+ consecutive days of blocking and the annual number of days of extreme (P90) and very extreme (P95) blocking is high over both domains (not shown). Over and to the east of the Antarctic Peninsula (90°–30°W domain), the correlation between the number of events of 4+ consecutive days of extreme blocking and the number of days of blocking (P90) decreases a bit in comparison with events of 2+ consecutive days. The latter could be related to the fact that the RAP pattern shows a lower persistence of consecutive days than LWS and LAB patterns (Table 2 in Gonzalez et al. 2018) and most of the blocking days in the 90°–30°W domain occur during the RAP pattern. The strong correlation between instantaneous days of blocking and multiday blocking events in both domains support the use of P90, P95, and P99 to characterize blocking episodes over the Antarctic Peninsula, despite those indices not considering blocking over more than one day.

The number of events with 2+ consecutive days of extreme blocking (P90) changes from the first period (1979–98) to the second (1999–2018) in both domains of this study (Figs. 12a,b). The number of blocking events decreases in the second 20-yr period for all seasons in the 150°–90°W domain (Fig. 12a). This is in agreement with the reduction in the number of days of extreme blocking (P90) shown in Table 4. When the above analysis is applied to P90 and P95 blocking events with 4+ consecutive days, the trends in the 150°–90°W domain are similar to that of blocking events with 2+ consecutive days (Figs. 13a,c). In the

TABLE 5. Percent of days with P90, P95, and P99 blocking over the 90°–30°W domain for the 1979–98 and 1999–2018 periods.

	1979–98			1999–2018		
Season percentile	P90	P95	P99	P90	P95	P99
DJF	54.6	59.7	70.3	45.4	40.3	29.7
MAM	45.9	44.0	32.4	54.1	56.0	67.6
JJA	47.6	47.3	37.8	52.4	52.7	62.2
SON	42.3	40.1	35.1	57.7	59.9	64.9

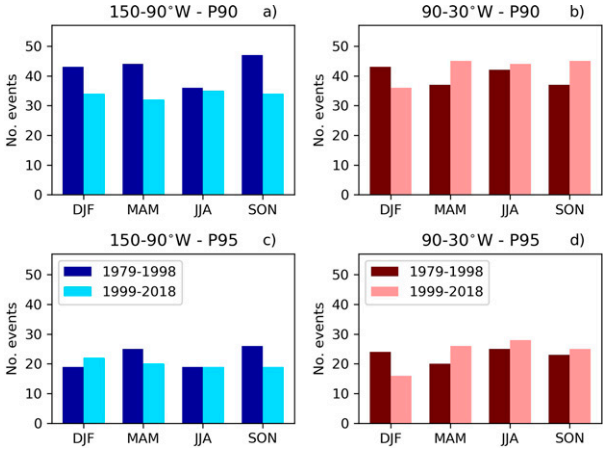

FIG. 12. Number of events defined as 2+ consecutive days of (a),(b) extreme blocking (P90) and (c),(d) very extreme blocking (P95) by season for the periods 1979–98 and 1999–2018 for the (left) 150°–90°W and (right) 90°–30°W domains.

90°–30°W domain, the trends in the number of 4+ consecutive days of blocking are similar to those in the number of 2+ consecutive days of blocking (Figs. 13b,d). These differences, however, could be related to multidecadal variability. Therefore, an in-depth analysis needs to be further carried out to better understand whether blocking events are becoming more frequent over the 90°–30°W than those over the 150°–90°W domain. In addition, since the number of P99 days shows the largest reduction in DJF (see Table 5), the reduction in the number of blocking events with 4+ consecutive days in DJF may be associated with a reduction of days with the most intense ridging.

d. Relation with the AAO

The AAO is a significant modulator of circulation in the middle and high southern latitudes (Gong and Wang 1999), so it is important to test its relationship to blocking. Extreme (P90) and very extreme (P95 and P99) blocking days in the 150°–90°W domain are much more likely on days with negative AAO than

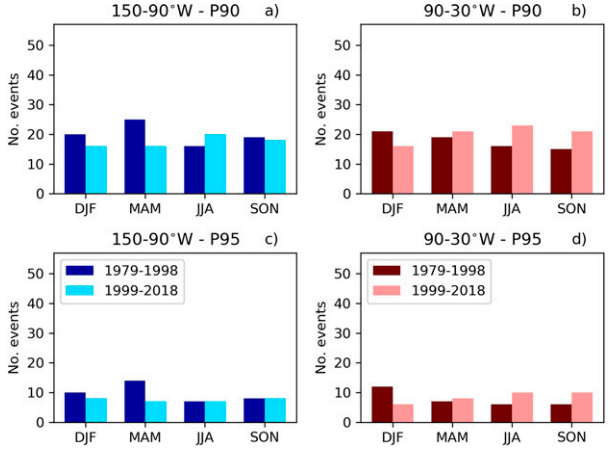

FIG. 13. As in Fig. 12, but for events of 4+ consecutive days.

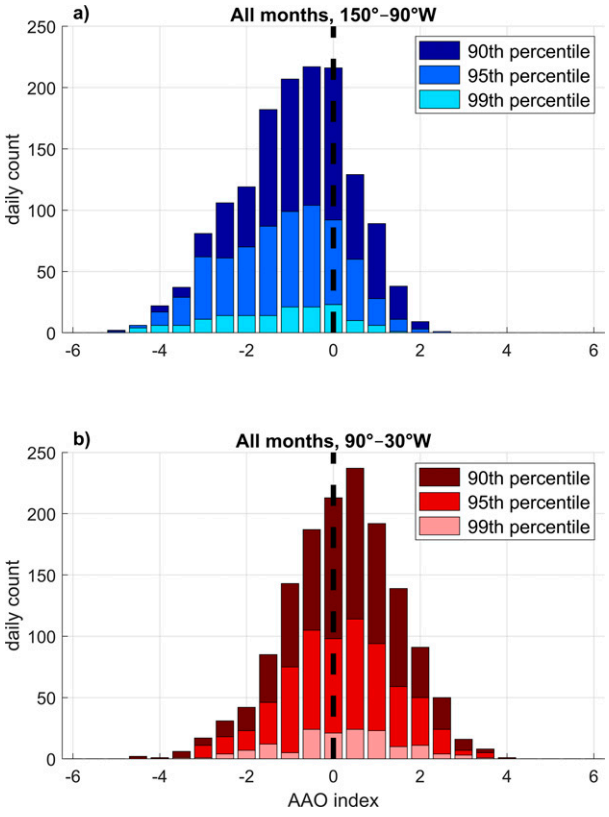

FIG. 14. Occurrences of extreme blocking (P90, P95, and P99) by value of the Antarctic Oscillation index for the (a) 150°–90°W and (b) 90°–30°W domains, from 1979 to 2018.

when it is positive: 74.5% of P90 days, 80.2% of P95 days, and 86.8% of P99 days occur when the AAO is negative (Fig. 14a). In the 90°–30°W domain, the relationship is reversed (although not as strong), and blocking there is more frequent when the AAO is positive: 57.4% of P90 days, 55.7% of P95 days, and 57.6% of P99 days occur when the AAO is positive. This relationship between the AAO and blocking to the south of South America agrees with Damião Mendes and Cavalcanti (2014), who found more instances of blocking in the southeastern Pacific Ocean when the AAO was negative and in the South Atlantic Ocean when the AAO was positive. Indeed, a negative AAO increases the occurrences of the LWS and LDP patterns of Gonzalez et al. (2018), and we found that for the 150°–90°W domain, blocking was most frequent during those two synoptic patterns (Fig. 5). Similarly, a positive AAO increases the occurrence of the LAB pattern (but not the RAP one), and we found greatest instances of blocking in the 90°–30°W domain during the LAB and RAP patterns (Fig. 8).

Variations in the phase of the AAO can influence pressure anomalies, which in turn lead to deepening of cyclonic systems and the development of blocking patterns. More frequent blocking days in the 150°–90°W domain during the negative phase of AAO is consistent with Turner et al. (2013b), who examined monthly trends in the absolute depth and location of the Amundsen Sea low and highlighted a

weakening trend in the Amundsen Sea low that appeared to be linked with the negative AAO. Emanuelsson et al. (2018) found the greatest geopotential height variability linked to the AAO in the Amundsen–Bellingshausen Sea, which corresponds to our western domain (150°–90°W), thus helping to explain why the link between the AAO and blocking was stronger in that domain than in the eastern one (90°–30°W). This agrees well with the work of Fogt et al. (2012), who studied trends in zonal asymmetries in the AAO, and here, the zonal AAO asymmetries could be placed where blocking is more likely to occur. They noted that zonal asymmetries in the AAO were most common in austral winter and spring and found that temperature variations in the Antarctic Peninsula are strongly tied to these asymmetries. They finally note that the asymmetries in the AAO were linked to the El Niño–Southern Oscillation (ENSO); the possible connections between blocking around the Antarctic Peninsula and ENSO are left for a further study.

Rather than simultaneous synoptic patterns, global and hemispheric modes of atmospheric teleconnection patterns can also have a considerable influence on regional circulation patterns. In this respect, tropical sea surface temperature and convection variability can create a wave source in the subtropics that excites quasi-stationary wave trains traveling poleward, which in turn can lead to major changes in regional circulation patterns around the Antarctic Peninsula (Yuan et al. 2018; Goyal et al. 2021). For instance, Rossby wave trains emanating from the central Pacific Ocean during El Niño and Madden–Julian oscillation events can lead to anomalous high sea level pressure and increased blocking patterns across the southeast Pacific and Antarctic Peninsula (Yuan and Martinson 2001; Steig et al. 2012; Yuan et al. 2018; Rondanelli et al. 2019).

4. Discussion and conclusions

In this study, we analyze atmospheric blocking patterns using a method of 500-hPa geopotential heights exceeding the 90th, 95th, and 99th percentiles. The analysis was conducted using data from the ERA-Interim reanalysis over two quasi-rectangular regions to the south of South America and north of Antarctica, bounded by latitudes 50°–70°S, and longitudes 150°–90°W (western domain) and 90°–30°W (eastern domain) (Fig. 1a). We compared our method with a more sophisticated hemispheric-scale blocking index (Tibaldi and Molteni 1990; Tibaldi et al. 1994). Overall, despite some differences, our method has notable agreement with that of Tibaldi, thus allowing for simplicity in the analysis of extreme blocking around the Antarctic Peninsula. It is important to note that while the method used to calculate the blocking indices in this study is mathematically simple, the physical processes involved in blocking are often complex.

Blocking west of the Antarctic Peninsula (150°–90°W domain) occurs mainly in association with a low over the Weddell Sea (LWS) (Gonzalez et al. 2018). That synoptic situation corresponds to anticyclonic conditions over the 150°–90°W domain. Over this region, blocking also occurs most frequently when the AAO is negative. Over and to the east of the Antarctic Peninsula (90°–30°W domain), a low over the Amundsen and Bellingshausen Seas (LAB) and a ridge over the Antarctic Peninsula (RAP) are the synoptic conditions (adopted from Gonzalez et al. 2018) more frequently associated with blocking. Over this region, blocking is more frequent when the AAO is positive. Given the potential linkage between some episodic extreme meteorological events and blocking patterns around the Antarctic Peninsula (e.g., Bozkurt et al. 2018; Rondanelli et al. 2019), these results may be useful in understanding extreme events in and around the peninsula.

Mean 500-hPa geopotential heights were statistically significantly different (using a Kolmogorov–Smirnov test) between 1979–98 and 1999–2018 in several seasons in both domains. However, because long-term trends over the 40-yr (1979–2018) period (using a Mann–Kendall test) were not statistically significant (except for a small trend in DJF in the 90°–30°W domain), we believe this is evidence of multidecadal variability in geopotential heights around the Antarctic Peninsula.

The number of days with blocking above the 90th percentile (P90) decreased from the 1979–98 to the 1999–2018 period during all seasons over the 150°–90°W domain, although this decrease was not statistically significant. The frequency of extreme blocking over the eastern domain (90°–30°W) decreased in DJF in the second 20-yr period relative to the first, particularly for the most extreme cases (however, not statistically significant). This agrees with a statistically significant negative long-term trend (using a Mann–Kendall test) in the mean geopotential height over the 90°–30°W domain. On the other hand, blocking in the eastern domain is more common from 1999 to 2018 than from 1979 to 1998 during the rest of the year, although these changes neither are statistically significant. In addition, long-term (1979–2018) trends in the number of blocking days were not statistically significant for any domain nor season of analysis. Due to the lack of statistical significance, a more in-depth analysis would be needed to better determine whether blocking days or events in the region are associated with multidecadal variability. Possible causes for the observed differences may also include temperature changes within the column affecting geopotential height and changes in the synoptic flow. Finally, it is important to mention that these changes in blocking days may be dependent on the gridded product, the period and region of analysis, and the index used (Barnes et al. 2014; Horton et al. 2015; Hanna et al. 2016; Woollings et al. 2018).

Recent studies have found a temperature decrease in the Antarctic Peninsula from the middle of the 1990s to the second half of 2010s (Gonzalez and Fortuny 2018; Jones et al. 2019; Turner et al. 2016; Bozkurt et al. 2020). This cooling was most pronounced in DJF and also statistically significant. In this study, we found a decrease in the number of blocking days in DJF for the eastern domain, although it was not statistically significant. In parallel to our findings, an increase of cyclonic circulations over and to the east of the peninsula (similar to our eastern domain) was found to trigger cold air advection from the continent to the peninsula (Turner et al. 2016). A work is currently under way to investigate the possible link between a decrease in blocking days in the 90°–30°W domain and the temperature decrease in the peninsula in recent decades.

Variability in the frequency of days with extreme blocking and multiday blocking events showed similar results. For this reason, we propose that our extreme blocking index can be used to indicate and analyze atmospheric blocking affecting

Southern Hemisphere regions around the Antarctic Peninsula, similar to how the Greenland Blocking Index has been used to diagnose blocking, its impacts, and its trends in the North Atlantic sector of the Arctic. Impacts on moisture transport and surface climate patterns may depend on whether blocking occurs to the west or to the east of the Antarctic Peninsula. Current work is under way to assess the seasonal and annual influences of extreme blocking patterns depicted in this study on the surface climate of the Antarctic Peninsula.

More research is needed to assess whether global climate models are able to capture extreme blocking patterns over the Antarctic Peninsula. For example, global climate models can contain persistent systematic errors in the present climate and future projections over the West Antarctica and Antarctic Peninsula, mostly controlled by large-scale features and sea ice feedbacks (e.g., Turner et al. 2013a; Wilson et al. 2016; Marshall et al. 2017). Moreover, synoptic-scale patterns such as anticyclonic and cyclonic conditions over the Antarctic Peninsula can lead to important model-to-model differences in climate change projections (Bozkurt et al. 2021). Additional studies are needed to further investigate this possibility.

Acknowledgments. Authors Marín and Bozkurt acknowledge support from Centro de Estudios Atmosféricos y Astroestadística (CEAAS), Universidad de Valparaíso. Bozkurt acknowledges support from ANID/CONICYT (Grant 77190080), ANID/PIA/Anillo INACH ACT192057 and ANID/FONDECYT/1120 0101, and COPAS COASTAL ANID FB210021. Author Barrett acknowledges the support of the Comisión Nacional de Investigación Científica y Tecnológica (CONICYT) in award MEC80180038.

REFERENCES

Barnes, E. A., and D. L. Hartmann, 2010: Influence of eddy-driven jet latitude on North Atlantic jet persistence and blocking frequency in CMIP3 integrations. *Geophys. Res. Lett.*, **37**, L23802, https://doi.org/10.1029/2010GL045700.

——, E. Dunn-Sigouin, G. Masato, and T. Woollings, 2014: Exploring recent trends in Northern Hemisphere blocking. *Geophys. Res. Lett.*, **41**, 638–644, https://doi.org/10.1002/2013GL058745.

Barrett, B. S., G. R. Henderson, E. McDonnell, M. Henry, and T. Mote, 2020: Extreme Greenland blocking and high-latitude moisture transport. *Atmos. Sci. Lett.*, **21**, e1002, https://doi.org/10.1002/asl.1002.

Barriopedro, D., R. García-Herrera, A. R. Lupo, and E. Hernández, 2006: A climatology of Northern Hemisphere blocking. *J. Climate*, **19**, 1042–1063, https://doi.org/10.1175/JCLI3678.1.

Berrisford, P., B. Hoskins, and E. Tyrlis, 2007: Blocking and Rossby wave breaking on the dynamical tropopause in the Southern Hemisphere. *J. Atmos. Sci.*, **64**, 2881–2898, https://doi.org/10.1175/JAS3984.1.

Black, E., M. Blackburn, G. Harrison, B. Hoskins, and J. Methven, 2004: Factors contributing to the summer 2003 European heatwave. *Weather*, **59**, 217–223, https://doi.org/10.1256/wea.74.04.

Bozkurt, D., R. Rondanelli, J. Marin, and R. Garreaud, 2018: Foehn event triggered by an atmospheric river underlies record-setting temperature along continental Antarctica. *J. Geophys. Res. Atmos.*, **123**, 3871–3892, https://doi.org/10.1002/2017JD027796.

——, D. H. Bromwich, J. Carrasco, K. M. Hines, J. C. Maureira, and R. Rondanelli, 2020: Recent near-surface temperature trends in the Antarctic Peninsula from observed, reanalysis and regional climate model data. *Adv. Atmos. Sci.*, **37**, 477–493, https://doi.org/10.1007/s00376-020-9183-x.

——, ——, ——, and R. Rondanelli, 2021: Temperature and precipitation projections for the Antarctic Peninsula over the next two decades: Contrasting global and regional climate model simulations. *Climate Dyn.*, **56**, 3853–3874, https://doi.org/10.1007/s00382-021-05667-2.

Bracegirdle, T. J., 2013: Climatology and recent increase of westerly winds over the Amundsen Sea derived from six reanalyses. *Int. J. Climatol.*, **33**, 843–851, https://doi.org/10.1002/joc.3473.

Bromwich, D. H., J. P. Nicolas, and A. J. Monaghan, 2011: An assessment of precipitation changes over Antarctica and the Southern Ocean since 1989 in contemporary global reanalyses. *J. Climate*, **24**, 4189–4209, https://doi.org/10.1175/2011JCLI4074.1.

Buehler, T., C. C. Raible, and T. F. Stocker, 2011: The relationship of winter season North Atlantic blocking frequencies to extreme cold or dry spells in the ERA-40. *Tellus*, **63A**, 174–187, https://doi.org/10.1111/j.1600-0870.2010.00492.x.

Carrasco, J. F., D. Bozkurt, and R. R. Cordero, 2021: A review of the observed air temperature in the Antarctic Peninsula. Did the warming trend come back after the early 21st hiatus? *Polar Sci.*, **28**, 100653, https://doi.org/10.1016/j.polar.2021.100653.

Cheng, X., and J. M. Wallace, 1993: Cluster analysis of the Northern Hemisphere wintertime 500-hpa height field: Spatial patterns. *J. Atmos. Sci.*, **50**, 2674–2696, https://doi.org/10.1175/1520-0469(1993)050<2674:CAOTNH>2.0.CO;2.

Clem, K. R., and R. L. Fogt, 2013: Varying roles of ENSO and SAM on the Antarctic Peninsula climate in austral spring. *J. Geophys. Res. Atmos.*, **118**, 11 481–11 492, https://doi.org/10.1002/jgrd.50860.

——, M. MacFerring, D. Kennett, D. Bozkurt, and T. Scambos, 2021: Record warmth and surface melt on the Antarctic Peninsula in February 2020 [in "State of the Climate in 2020"]. *Bull. Amer. Meteor. Soc.*, **102** (8), S328–S329, https://doi.org/10.1175/2021BAMSStateoftheClimate.1.

Damião Mendes, M. C., and I. F. A. Cavalcanti, 2014: The relationship between the Antarctic oscillation and blocking events over the South Pacific and Atlantic Oceans. *Int. J. Climatol.*, **34**, 529–544, https://doi.org/10.1002/joc.3729.

Davini, P., C. Cagnazzo, S. Gualdi, and A. Navarra, 2012: Bidimensional diagnostics, variability, and trends of Northern Hemisphere blocking. *J. Climate*, **25**, 6496–6509, https://doi.org/10.1175/JCLI-D-12-00032.1.

——, ——, P. G. Fogli, E. Manzini, S. Gualdi, and A. Navarra, 2014: European blocking and Atlantic jet stream variability in the NCEP/NCAR reanalysis and the CMCC-CMS climate model. *Climate Dyn.*, **43**, 71–85, https://doi.org/10.1007/s00382-013-1873-y.

——, A. Weisheimer, M. Balmaseda, S. J. Johnson, F. Molteni, C. D. Roberts, R. Senan, and T. N. Stockdale, 2021: The representation of winter Northern Hemisphere atmospheric blocking in ECMWF seasonal prediction systems. *Quart. J. Roy. Meteor. Soc.*, **147**, 1344–1363, https://doi.org/10.1002/qj.3974.

Dee, D. P., and Coauthors, 2011: The ERA-Interim reanalysis: Configuration and performance of the data assimilation system. *Quart. J. Roy. Meteor. Soc.*, **137**, 553–597, https://doi.org/10.1002/qj.828.

de Lima Nascimento, E., and T. Ambrizzi, 2002: The influence of atmospheric blocking on the Rossby wave propagation in Southern Hemisphere winter flows. *J. Meteor. Soc. Japan*, **80**, 139–159, https://doi.org/10.2151/jmsj.80.139.

Ding, Q., E. J. Steig, D. S. Battisti, and J. M. Wallace, 2012: Influence of the tropics on the southern annular mode. *J. Climate*, **25**, 6330–6348, https://doi.org/10.1175/JCLI-D-11-00523.1.

Dole, R. M., and N. D. Gordon, 1983: Persistent anomalies of the extratropical Northern Hemisphere wintertime circulation: Geographical distribution and regional persistence characteristics. *Mon. Wea. Rev.*, **111**, 1567–1586, https://doi.org/10.1175/1520-0493(1983)111<1567:PAOTEN>2.0.CO;2.

——, and Coauthors, 2011: Was there a basis for anticipating the 2010 Russian heat wave? *Geophys. Res. Lett.*, **38**, L06702, https://doi.org/10.1029/2010GL046582.

Emanuelsson, B. D., N. A. Bertler, P. D. Neff, J. A. Renwick, B. R. Markle, W. T. Baisden, and E. D. Keller, 2018: The role of Amundsen–Bellingshausen Sea anticyclonic circulation in forcing marine air intrusions into west Antarctica. *Climate Dyn.*, **51**, 3579–3596, https://doi.org/10.1007/s00382-018-4097-3.

Fang, Z., 2004: Statistical relationship between the Northern Hemisphere sea ice and atmospheric circulation during wintertime. *Observation, Theory and Modeling of Atmospheric Variability: Selected Papers of Nanjing Institute of Meteorology Alumni in Commemoration of Professor Jijia Zhang*, World Scientific, 131–141.

Fogt, R. L., J. M. Jones, and J. Renwick, 2012: Seasonal zonal asymmetries in the southern annular mode and their impact on regional temperature anomalies. *J. Climate*, **25**, 6253–6270, https://doi.org/10.1175/JCLI-D-11-00474.1.

Gong, D., and S. Wang, 1999: Definition of Antarctic oscillation index. *Geophys. Res. Lett.*, **26**, 459–462, https://doi.org/10.1029/1999GL900003.

Gonzalez, S., and D. Fortuny, 2018: How robust are the temperature trends on the Antarctic Peninsula? *Antarct. Sci.*, **30**, 322–328, https://doi.org/10.1017/S0954102018000251.

——, F. Vasallo, C. Recio-Blitz, J. A. Guijarro, and J. Riesco, 2018: Atmospheric patterns over the Antarctic Peninsula. *J. Climate*, **31**, 3597–3608, https://doi.org/10.1175/JCLI-D-17-0598.1.

Goyal, R., M. Jucker, A. Sen Gupta, and M. H. England, 2021: Generation of the Amundsen Sea low by Antarctic orography. *Geophys. Res. Lett.*, **48**, e2020GL091487, https://doi.org/10.1029/2020GL091487.

Häkkinen, S., P. B. Rhines, and D. L. Worthen, 2011: Atmospheric blocking and Atlantic multi-decadal ocean variability. *Science*, **334**, 655–659, https://doi.org/10.1126/science.1205683.

Hanna, E., J. M. Jones, J. Cappelen, S. H. Mernild, L. Wood, K. Steffen, and P. Huybrechts, 2013: The influence of North Atlantic atmospheric and oceanic forcing effects on 1900-2010 Greenland summer climate and ice melt/runoff. *Int. J. Climatol.*, **33**, 862–880, https://doi.org/10.1002/joc.3475.

——, and Coauthors, 2014: Atmospheric and oceanic climate forcing of the exceptional Greenland ice sheet surface melt in summer 2012. *Int. J. Climatol.*, **34**, 1022–1037, https://doi.org/10.1002/joc.3743.

——, T. E. Cropper, P. D. Jones, A. A. Scaife, and R. Allan, 2015: Recent seasonal asymmetric changes in the NAO (a marked summer decline and increased winter variability) and associated changes in the AO and Greenland Blocking Index. *Int. J. Climatol.*, **35**, 2540–2554, https://doi.org/10.1002/joc.4157.

——, ——, R. J. Hall, and J. Cappelen, 2016: Greenland Blocking Index 1851–2015: A regional climate change signal. *Int. J. Climatol.*, **36**, 4847–4861, https://doi.org/10.1002/joc.4673.

——, R. J. Hall, T. E. Cropper, T. J. Ballinger, L. Wake, T. Mote, and J. Cappelen, 2018: Greenland blocking index daily series 1851–2015: Analysis of changes in extremes and links with North Atlantic and UK climate variability and change. *Int. J. Climatol.*, **38**, 3546–3564, https://doi.org/10.1002/joc.5516.

Hirasawa, N., H. Nakamura, H. Motoyama, M. Hayashi, and T. Yamanouchi, 2013: The role of synoptic-scale features and advection in prolonged warming and generation of different forms of precipitation at Dome Fuji station, Antarctica, following a prominent blocking event. *J. Geophys. Res. Atmos.*, **118**, 6916–6928, https://doi.org/10.1002/jgrd.50532.

Horton, D. E., N. C. Johnson, D. Singh, D. L. Swain, B. Rajaratnam, and N. S. Diffenbaugh, 2015: Contribution of changes in atmospheric circulation patterns to extreme temperature trends. *Nature*, **522**, 465–469, https://doi.org/10.1038/nature14550.

Hosking, J. S., A. Orr, G. J. Marshall, J. Turner, and T. Phillips, 2013: The influence of the Amundsen–Bellingshausen Seas low on the climate of West Antarctica and its representation in coupled climate model simulations. *J. Climate*, **26**, 6633–6648, https://doi.org/10.1175/JCLI-D-12-00813.1.

Hoskins, B. J., and P. D. Sardeshmukh, 1987: A diagnostic study of the dynamics of the Northern Hemisphere winter of 1985-86. *Quart. J. Roy. Meteor. Soc.*, **113**, 759–778, https://doi.org/10.1002/qj.49711347705.

Jones, M. E., D. H. Bromwich, J. P. Nicolas, J. Carrasco, E. Plavcová, X. Zou, and S.-H. Wang, 2019: Sixty years of widespread warming in the southern middle and high latitudes (1957–2016). *J. Climate*, **32**, 6875–6898, https://doi.org/10.1175/JCLI-D-18-0565.1.

Jones, R. W., I. Renfrew, A. Orr, B. Webber, D. Holland, and M. Lazzara, 2016: Evaluation of four global reanalysis products using in situ observations in the Amundsen Sea Embayment, Antarctica. *J. Geophys. Res. Atmos.*, **121**, 6240–6257, https://doi.org/10.1002/2015JD024680.

Kennedy, D., T. Parker, T. Woollings, B. Harvey, and L. Shaffrey, 2016: The response of high impact blocking weather systems to climate change. *Geophys. Res. Lett.*, **43**, 7250–7258, https://doi.org/10.1002/2016GL069725.

King, J. C., and J. Turner, 2009: *Antarctic Meteorology and Climatology*. Cambridge University Press, 424 pp.

Legras, B., and M. Ghil, 1985: Persistent anomalies, blocking and variations in atmospheric predictability. *J. Atmos. Sci.*, **42**, 433–471, https://doi.org/10.1175/1520-0469(1985)042<0433:PABAVI>2.0.CO;2.

LejenÄs, H., and H. Økland, 1983: Characteristics of Northern Hemisphere blocking as determined from a long time series of observational data. *Tellus*, **35A**, 350–362, https://doi.org/10.3402/tellusa.v35i5.11446.

Marshall, G. J., D. W. J. Thompson, and M. R. Van den Broeke, 2017: The signature of Southern Hemisphere atmospheric circulation patterns in Antarctic precipitation. *Geophys. Res. Lett.*, **44**, 11 580–11 589, https://doi.org/10.1002/2017GL075998.

Masato, G., B. J. Hoskins, and T. Woollings, 2013: Winter and summer Northern Hemisphere blocking in CMIP5 models. *J. Climate*, **26**, 7044–7059, https://doi.org/10.1175/JCLI-D-12-00466.1.

Mattingly, K., T. Mote, and X. Fettweis, 2018: Atmospheric river impacts on Greenland Ice Sheet surface mass balance.

J. Geophys. Res. Atmos., **123**, 8538–8560, https://doi.org/10.1029/2018JD028714.

Meehl, G., A. Hu, and H. Teng, 2016: Initialized decadal prediction for transition to positive phase of the interdecadal Pacific oscillation. *Nat. Commun.*, **7**, 11718, https://doi.org/10.1038/ncomms11718.

Michelangeli, P.-A., R. Vautard, and B. Legras, 1995: Weather regimes: Recurrence and quasistationarity. *J. Atmos. Sci.*, **52**, 1237–1256, https://doi.org/10.1175/1520-0469(1995)052<1237:WRRAQS>2.0.CO;2.

Mo, K. C., 2000: Relationships between low-frequency variability in the Southern Hemisphere and sea surface temperature anomalies. *J. Climate*, **13**, 3599–3610, https://doi.org/10.1175/1520-0442(2000)013<3599:RBLFVI>2.0.CO;2.

Nabizadeh, E., P. Hassanzadeh, D. Yang, and E. A. Barnes, 2019: Size of the atmospheric blocking events: Scaling law and response to climate change. *Geophys. Res. Lett.*, **46**, 13 488–13 499, https://doi.org/10.1029/2019GL084863.

Ndarana, T., and D. W. Waugh, 2011: A climatology of Rossby wave breaking on the Southern Hemisphere tropopause. *J. Atmos. Sci.*, **68**, 798–811, https://doi.org/10.1175/2010JAS3460.1.

Neff, W., 2018: Atmospheric rivers melt Greenland. *Nat. Climate Change*, **8**, 857–858, https://doi.org/10.1038/s41558-018-0297-4.

O'Kane, T. J., J. S. Risbey, C. Franzke, I. Horenko, and D. P. Monselesan, 2013: Changes in the metastability of the midlatitude Southern Hemisphere circulation and the utility of nonstationary cluster analysis and split-flow blocking indices as diagnostic tools. *J. Atmos. Sci.*, **70**, 824–842, https://doi.org/10.1175/JAS-D-12-028.1.

Oliva, M., F. Navarro, F. Hrbacek, A. Hernandez, D. Nyvlt, P. Pereira, J. Ruiz-Fernandez, and R. Trigo, 2017: Recent regional climate cooling on the Antarctic Peninsula and associated impacts on the cryosphere. *Sci. Total Environ.*, **580**, 210–223, https://doi.org/10.1016/j.scitotenv.2016.12.030.

Parker, T. J., G. J. Berry, and M. J. Reeder, 2014: The structure and evolution of heat waves in southeastern Australia. *J. Climate*, **27**, 5768–5785, https://doi.org/10.1175/JCLI-D-13-00740.1.

Patterson, M., T. Bracegirdle, and T. Woollings, 2019: Southern Hemisphere atmospheric blocking in CMIP5 and future changes in the Australia-New Zealand sector. *Geophys. Res. Lett.*, **46**, 9281–9290, https://doi.org/10.1029/2019GL083264.

Pelly, J. L., and B. J. Hoskins, 2003: A new perspective on blocking. *J. Atmos. Sci.*, **60**, 743–755, https://doi.org/10.1175/1520-0469(2003)060<0743:ANPOB>2.0.CO;2.

Pfahl, S., and H. Wernli, 2012: Quantifying the relevance of atmospheric blocking for co-located temperature extremes in the Northern Hemisphere on (sub-) daily time scales. *Geophys. Res. Lett.*, **39**, L12807, https://doi.org/10.1029/2012GL052261.

Pook, M., J. Risbey, P. Mclntosh, C. Ummenhofer, A. Marshall, and G. Meyers, 2013: The seasonal cycle of blocking and associated physical mechanisms in the Australian region and relationship with rainfall. *Mon. Wea. Rev.*, **141**, 4534–4553, https://doi.org/10.1175/MWR-D-13-00040.1.

Raphael, M. N., and Coauthors, 2016: The Amundsen Sea low: Variability, change, and impact on Antarctic climate. *Bull. Amer. Meteor. Soc.*, **97**, 111–121, https://doi.org/10.1175/BAMS-D-14-00018.1.

Rasmusson, E. M., and J. M. Wallace, 1983: Meteorological aspects of the El Niño/Southern Oscillation. *Science*, **222**, 1195–1202, https://doi.org/10.1126/science.222.4629.1195.

Reeder, M. J., T. Spengler, and R. Musgrave, 2015: Rossby waves, extreme fronts, and wildfires in southeastern Australia. *Geophys. Res. Lett.*, **42**, 2015–2023, https://doi.org/10.1002/2015GL063125.

Renwick, J. A., 1998: ENSO-related variability in the frequency of South Pacific blocking. *Mon. Wea. Rev.*, **126**, 3117–3123, https://doi.org/10.1175/1520-0493(1998)126<3117:ERVITF>2.0.CO;2.

——, 2002: Southern Hemisphere circulation and relations with sea ice and sea surface temperature. *J. Climate*, **15**, 3058–3068, https://doi.org/10.1175/1520-0442(2002)015<3058:SHCARW>2.0.CO;2.

——, 2005: Persistent positive anomalies in the Southern Hemisphere circulation. *Mon. Wea. Rev.*, **133**, 977–988, https://doi.org/10.1175/MWR2900.1.

Rex, D. F., 1950a: Blocking action in the middle troposphere and its effect upon regional climate. *Tellus*, **3**, 196–211, https://doi.org/10.1111/j.2153-3490.1950.tb00331.x.

——, 1950b: Blocking action in the middle troposphere and its effect upon regional climate. Part II: The climatology of blocking action. *Tellus*, **3**, 275–301, https://doi.org/10.3402/tellusa.v2i4.8603.

Rodrigues, R. R., and T. Woollings, 2017: Impact of atmospheric blocking on South America in austral summer. *J. Climate*, **30**, 1821–1837, https://doi.org/10.1175/JCLI-D-16-0493.1.

Rondanelli, R., B. Hatchett, J. Rutllant, D. Bozkurt, and R. Garreaud, 2019: Strongest MJO on record triggers extreme Atacama rainfall and warmth in Antarctica. *Geophys. Res. Lett.*, **46**, 3482–3491, https://doi.org/10.1029/2018GL081475.

Scaife, A. A., T. Woollings, J. Knight, G. Martin, and T. Hinton, 2010: Atmospheric blocking and mean biases in climate models. *J. Climate*, **23**, 6143–6152, https://doi.org/10.1175/2010JCLI3728.1.

Schaller, N., J. Sillmann, J. Anstey, E. M. Fischer, C. M. Grams, and S. Russo, 2018: Influence of blocking on northern European and western Russian heatwaves in large climate model ensembles. *Environ. Res. Lett.*, **13**, 054015, https://doi.org/10.1088/1748-9326/aaba55.

Scherrer, S. C., M. Croci-Maspoli, C. Schwierz, and C. Appenzeller, 2006: Two-dimensional indices of atmospheric blocking and their statistical relationship with winter climate patterns in the Euro-Atlantic region. *Int. J. Climatol.*, **26**, 233–249, https://doi.org/10.1002/joc.1250.

Shutts, G., 1986: A case study of eddy forcing during an Atlantic blocking episode. *Anomalous Atmospheric Flows and Blocking*, Advances in Geophysics, Vol. 29, Elsevier, 135–162, https://doi.org/10.1016/S0065-2687(08)60037-0.

Sillmann, J., M. Croci-Maspoli, M. Kallache, and R. W. Katz, 2011: Extreme cold winter temperatures in Europe under the influence of North Atlantic atmospheric blocking. *J. Climate*, **24**, 5899–5913, https://doi.org/10.1175/2011JCLI4075.1.

Sinclair, M. R., 1996: A climatology of anticyclones and blocking for the Southern Hemisphere. *Mon. Wea. Rev.*, **124**, 245–264, https://doi.org/10.1175/1520-0493(1996)124<0245:ACOAAB>2.0.CO;2.

Smyth, P., K. Ide, and M. Ghil, 1999: Multiple regimes in Northern Hemisphere height fields via mixture model clustering. *J. Atmos. Sci.*, **56**, 3704–3723, https://doi.org/10.1175/1520-0469(1999)056<3704:MRINHH>2.0.CO;2.

Stammerjohn, S., D. G. Martinson, R. C. Smith, X. Yuan, and D. Rind, 2008: Antarctic annual sea ice retreat and advance and their relation to El Niño-Southern Oscillation and southern annular mode variability. *J. Geophys. Res.*, **113**, C03S90, https://doi.org/10.1029/2007JC004269.

Steig, E. J., Q. Ding, D. Battisti, and A. Jenkins, 2012: Tropical forcing of circumpolar deep water inflow and outlet glacier thinning in the Amundsen Sea embayment, west Antarctica. *Ann. Glaciol.*, **53**, 19–28, https://doi.org/10.3189/2012AoG60A110.

Tang, M. S., S. N. Chenoli, S. Colwell, R. Grant, M. Simms, J. Law, and A. Abu Samah, 2018: Precipitation instruments at Rothera Station, Antarctic Peninsula: A comparative study. *Polar Res.*, **37**, 1503906, https://doi.org/10.1080/17518369.2018.1503906.

Thompson, D. W., and J. M. Wallace, 2000: Annular modes in the extratropical circulation. Part I: Month-to-month variability. *J. Climate*, **13**, 1000–1016, https://doi.org/10.1175/1520-0442(2000)013<1000:AMITEC>2.0.CO;2.

Tibaldi, S., and F. Molteni, 1990: On the operational predictability of blocking. *Tellus*, **42A**, 343–365, https://doi.org/10.3402/tellusa.v42i3.11882.

——, E. Tosi, A. Navarra, and L. Pedulli, 1994: Northern and Southern Hemisphere seasonal variability of blocking frequency and predictability. *Mon. Wea. Rev.*, **122**, 1971–2003, https://doi.org/10.1175/1520-0493(1994)122<1971:NASHSV>2.0.CO;2.

Trenberth, K. F., and K. C. Mo, 1985: Blocking in the Southern Hemisphere. *Mon. Wea. Rev.*, **113**, 3–21, https://doi.org/10.1175/1520-0493(1985)113<0003:BITSH>2.0.CO;2.

Turner, J., T. J. Bracegirdle, T. Phillips, G. J. Marshall, and J. S. Hosking, 2013a: An initial assessment of Antarctic sea ice extent in the CMIP5 models. *J. Climate*, **26**, 1473–1484, https://doi.org/10.1175/JCLI-D-12-00068.1.

——, T. Phillips, S. Hosking, G. J. Marshall, and A. Orr, 2013b: The Amundsen Sea low. *Int. J. Climatol.*, **33**, 1818–1829, https://doi.org/10.1002/joc.3558.

——, and Coauthors, 2016: Absence of 21st century warming on Antarctic Peninsula consistent with natural variability. *Nature*, **535**, 411–415, https://doi.org/10.1038/nature18645.

Tyrlis, E., and B. Hoskins, 2008: Aspects of a Northern Hemisphere atmospheric blocking climatology. *J. Atmos. Sci.*, **65**, 1638–1652, https://doi.org/10.1175/2007JAS2337.1.

Vautard, R., 1990: Multiple weather regimes over the North Atlantic: Analysis of precursors and successors. *Mon. Wea. Rev.*, **118**, 2056–2081, https://doi.org/10.1175/1520-0493(1990)118<2056:MWROTN>2.0.CO;2.

Wachowicz, L. J., J. R. Preece, T. L. Mote, B. S. Barrett, and G. R. Henderson, 2021: Historical trends of seasonal Greenland blocking under different blocking metrics. *Int. J. Climatol.*, **41** (Suppl. 1), E3263–E3278, https://doi.org/10.1002/joc.6923.

Wallace, J., 2000: On the Arctic and Antarctic oscillations. *2000 NCAR Advanced Studies Program Summer Colloquium on Dynamics of Decadal to Centennial Climate Variability*, Boulder, CO, NCAR, http://research.jisao.washington.edu/wallace/ncar_notes/#References.

Weijenborg, C., H. de Vries, and R. J. Haarsma, 2012: On the direction of Rossby wave breaking in blocking. *Climate Dyn.*, **39**, 2823–2831, https://doi.org/10.1007/s00382-012-1332-1.

Wiedenmann, J. M., A. R. Lupo, I. I. Mokhov, and E. A. Tikhonova, 2002: The climatology of blocking anticyclones for the Northern and Southern Hemispheres: Block intensity as a diagnostic. *J. Climate*, **15**, 3459–3473, https://doi.org/10.1175/1520-0442(2002)015<3459:TCOBAF>2.0.CO;2.

Wilson, A. B., D. H. Bromwich, and K. M. Hines, 2016: Simulating the mutual forcing of anomalous high Southern latitude atmospheric circulation by El Niño flavors and the southern annular mode. *J. Climate*, **29**, 2291–2309, https://doi.org/10.1175/JCLI-D-15-0361.1.

Woollings, T., B. Hoskins, M. Blackburn, and P. Berrisford, 2008: A new Rossby wave–breaking interpretation of the North Atlantic Oscillation. *J. Atmos. Sci.*, **65**, 609–626, https://doi.org/10.1175/2007JAS2347.1.

——, and Coauthors, 2018: Blocking and its response to climate change. *Curr. Climate Change Rep.*, **4**, 287–300, https://doi.org/10.1007/s40641-018-0108-z.

Wright, W., 1994: Seasonal climate summary Southern Hemisphere (autumn 1993)—A second mature ENSO phase. *Aust. Meteor. Mag.*, **43**, 205–212.

Yuan, X., and D. G. Martinson, 2001: The Antarctic dipole and its predictability. *Geophys. Res. Lett.*, **28**, 3609–3612, https://doi.org/10.1029/2001GL012969.

——, M. R. Kaplan, and M. A. Cane, 2018: The interconnected global climate system—A review of tropical–polar teleconnections. *J. Climate*, **31**, 5765–5792, https://doi.org/10.1175/JCLI-D-16-0637.1.